Beyond Traditional Hyperthermia. *In vivo* Cancer Treatment with Magnetic-Responsive Mesoporous Silica Nanocarriers

Eduardo Guisasola,[±] Laura Asín,[±] Lilianne Beola, Jesús M. de la Fuente, Alejandro Baeza and María Vallet-Regí**

Dr. E. Guisasola, Dr. A. Baeza and Prof. M. Vallet-Regí. Dpto. Química Inorgánica y Bioinorgánica, Facultad de Farmacia, UCM, Instituto de Investigación Sanitaria Hospital 12 de Octubre i+ 12, 28040 Madrid, Spain. Centro de Investigación Biomédica en Red de Bioingeniería, Biomateriales y Nanomedicina (CIBER-BBN), Avenida Monforte de Lemos, 3-5, 28029 Madrid, Spain.

Lilianne Beola, Dr. L. Asín and Dr. J. M. de la Fuente. Instituto de Ciencia de Materiales de Aragón (ICMA), CSIC/Universidad de Zaragoza, C/ Pedro Cerbuna 12, Zaragoza, Spain. Centro de Investigación Biomédica en Red de Bioingeniería, Biomateriales y Nanomedicina (CIBER-BBN), Avenida Monforte de Lemos, 3-5, 28029 Madrid, Spain.

[±] Both authors have contributed equally

Keywords: hot spot, stimuli-responsive, drug delivery, magnetic hyperthermia, synergic therapy, silica mesoporous nanoparticles, thermosensitive polymer

ABSTRACT

In this study we present an innovation in the tumor treatment *in vivo* mediated by magnetic mesoporous silica nanoparticles (MMSNs). This device was built with iron oxide magnetic nanoparticles embedded in a mesoporous silica matrix and coated with an engineered thermoresponsive polymer. The magnetic nanoparticles act as internal heating sources under an alternating magnetic field (AMF) that increase the temperature of the surroundings, provoking the polymer transition and consequently the release of a drug trapped inside the silica pores. By a synergic effect between the intracellular hyperthermia and chemotherapy triggered by AMF application, significant tumor growth inhibition was achieved in 48 hours after treatment. Furthermore, the small magnetic loading used in the experiments indicates that the treatment is carried out without a global temperature rise of the tissue, which avoids the problem of the necessity to employ large amounts of magnetic cores, as is common in current magnetic hyperthermia.

INTRODUCTION

The lack of selectivity of traditional chemotherapy towards tumor masses can cause serious side effects in patients due to the high toxicity of administered anticancer drugs. In addition, this poisonous restricts the dosage and diminishes the effectiveness of the treatments. Thanks to their nanometer size, the application of nanomaterials in oncology has been revealed as an important tool to improve the action of traditional chemotherapy agents in terms of specificity, security and bioavailability.[1] The preferential accumulation of nanocarriers in solid tumors is a consequence of the defective vasculature of cancer tissues derived from the fast growing of the blood vessels and enhanced by an inefficient lymphatic drainage, as was revealed by Maeda and Matsumura in

1986. This passive targeting is named enhanced permeation and retention effect (EPR effect).[2,3] One of the challenges of the nanomedicine nowadays is the development of drug delivery vehicles with stimuli-responsive properties in order to dispense on demand the transported therapeutic agents, reducing the side toxicity and enhancing the solubility and circulation time of housed drugs.[4–7] Retaining the cytotoxic agents inside the nanocarrier during its travel to the cancer tissue, the systemic toxicity of the anticancer drugs can be avoided or decreased which results in a significant reduction of the side effects of the treatment. Once the accumulation in the tumoral mass has occurred, the presence of certain stimuli fires the triggering mechanism provoking the drug departure and consequently, the cancer cell death in a highly localized area. Among this field, mesoporous silica nanoparticles (MSNs) have great properties to build stimuli-responsive drug delivery devices, as high surface area where large amounts of drugs can be hosted, ease functionalization of the inner and outer surface by silanol chemistry, and high chemical stability.[8,9] Different stimuli such as ultrasounds, light, pH, enzymes and others, can be used to trigger the drug release from the nanocarrier.[10–17] Therefore, it is possible to develop specific treatments for the target disease choosing the stimuli that is more convenient depending on the pathology characteristics that have to be treated.[18] Magnetic fields are non-invasive stimulus and possesses a high penetration in tissues which represents an exceptional opportunity to develop magnetically triggered drug delivery devices.[19–27] To confer magnetic properties to the mesoporous silica nanodevices, the inclusion of magnetic nanoparticles (MNPs) in the nanocarriers is mandatory to take advantage of its interactions with magnetic fields. These interactions lead to interesting possibilities as magnetic targeting through static magnetic fields,[28,29] magnetic protein separation[30] or the one that will be addressed in this study, the hyperthermia treatment with alternating magnetic fields (AMF). Hyperthermia have been proved

as an efficient treatment against tumors but, as any other technique, presents some drawbacks such as limitations of the AMF generation source or application parameters or the need to achieve high concentrations of MNPs in the target tissue.[31] At this point, some studies showed that it is possible to induce toxicity in cancer cells by hyperthermia, even when the released heat does not increase the macroscopic temperature, but it is still a matter of controversy despite of some examples showed by different authors.[32,33] After a literature examination, the published dual treatments combining hyperthermia and chemotherapy with a single nanocarrier, always needed a macroscopic temperature rise in order to cause the cancer growth inhibition or eradication.[34–36] This work presents an innovation in the tumor treatment *in vivo* mediated by magnetic mesoporous silica nanoparticles (MMSNs), by a synergic effect between the intracellular hyperthermia and chemotherapy triggered by AMF application. Furthermore, the small magnetic loading used in the experiments indicates that the treatment is carried out without a global temperature rise of the tissue.

To address this goal, superparamagnetic iron oxide nanoparticles (SPIONS) were first embedded in a mesoporous silica matrix and then, the external silica surface was coated with a thermosensitive polymer shell which acts as a gatekeeper of chemotherapeutic drugs trapped in the pore network. The AMF induces a change in the magnetic moment orientation inside the magnetic nanocrystals, that cause energy losses traduced in heat dissipation though the Néel relaxation mechanism.[20] The temperature rise inside the nanocarrier reaches the thermoresponsive polymer layer which suffers a hydrophilic to hydrophobic transition. The polymer shrinking creates open spaces in the polymer barrier that allows the drug departure to the cancer tissue at the same time that the heat shock produce the cell damage, making cells more sensitive to chemotherapeutic agents (Scheme 1).[37] Recently, our teams have demonstrated *in*

vitro the capacity of this nanodevice to release drugs under AMF exposition without the need to increase the temperature macroscopically.[38] However, the capability to trigger the delivery of small drugs under AMF within a living body was still untested in this kind of devices. This fact is even more exciting considering that the *in vivo* release was accomplished using low amounts of MNPs, which makes unnecessary to employ high doses of magnetic payload to trigger the drug release by increasing the macroscopic temperature in the cancer tissue.[31]

The novelty of this study is grounded in several facts as: (1) the first reported *in vivo* evaluation of magnetically-triggerable MSN based nanomaterial which can produce a heat shock that activates the polymeric gate within a tissue; (2) that release a potent cytotoxic compound as doxorubicin, that provokes a significant tumor growth inhibition in 48 h only when AMF was applied; (3) taking into account that this inhibition was achieved at low magnetic doses without a global temperature rise, which (4) proves the synergic effect of magnetic hyperthermia (MH) and chemotherapy. This device also showed a remarkably high tissue penetration and low toxicity without the AMF application, which are important properties for drug delivery nanocarriers. It is also relevant to consider that this device has many opportunities for the improvement, e. g. employing its magnetic targeting capability or the chemical attachment of active targeting moieties in its surface.

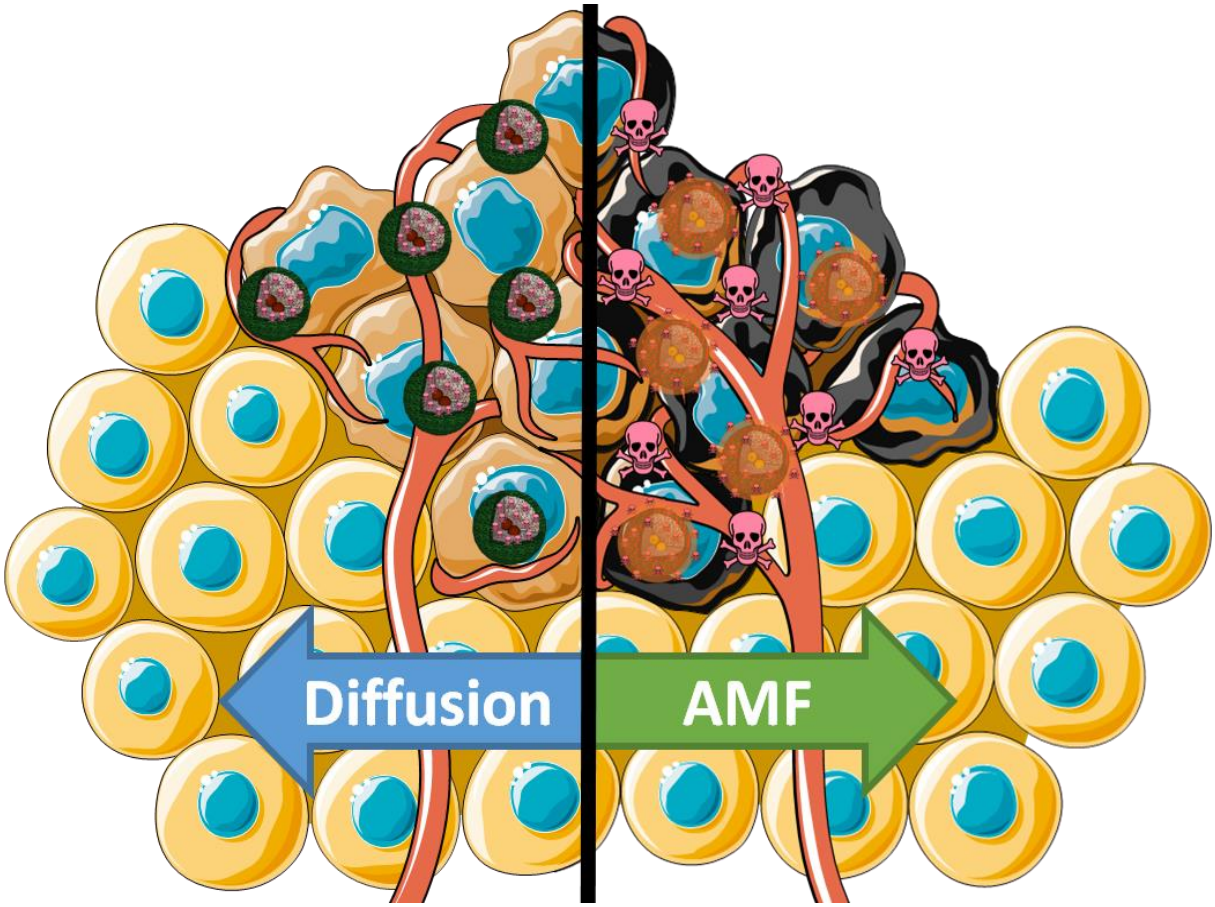

Scheme 1. The nanocarriers is diffused in the cancer tissue after intratumoral injection and release its drug cargo when AMF is applied, provoking the tumor cell death.

RESULTS AND DISCUSSION

The synthesis of MMSNs coated with the thermosensitive polymer has been carried out following a method previously reported by our group.[38] Briefly, SPIONs were synthesized by co-precipitation of iron chloride salts in the presence of oleic acid (OA), obtaining stable hydrophobic magnetic nanoparticles with 9 nm size distribution and superparamagnetic behavior. The SPIONS were transferred to aqueous media with hexadecyltrimethylammonium bromide (CTAB), which also acted as a structure directing agent in the silica growth step by adding TEOS dropwise in the SPION suspension at basic pH.[39] The silica surface was

functionalized *in situ* with small poly (ethylene glycol) chains to confer colloidal stability to the nanocarrier.[40] Straightaway the silica surface was decorated with polymerizable groups with 3-[tris(trimethylsiloxy)silyl]propyl methacrylate (MPS) and the CTAB surfactant was extracted by ion exchange to obtain MMSN-MPS precursor. Then, a radical polymerization was performed with *N*-isopropylacrylamide (NIPAM), *N*- (hydroxymethyl)acrylamide (NHMA) and *N, N'*-methylenebis(acrylamide) (MBA) monomers in the presence of MMSNPs and ammonium persulfate (APS) as radical initiator, obtaining a polymer shell on the nanoparticles surface (Scheme in **Figure 1**). The polymer shell was designed to have a lower critical solution temperature (LCST) at 42 ˚C by controlling the ratio between its two main monomers. The LCST is the transition temperature which the polymer suffers a change from hydrophilic to hydrophobic state. This fact means that below the LCST the polymer chains will form a mesh that blocks the pore openings keeping the drug inside the silica matrix. When the temperature on the nanocarrier surroundings overcomes the transition temperature, the polymer suffers a collapse creating gaps in its structure and therefore allowing the drug release.

Both, precursor MMSN-MPS and magnetic mesoporous nanocarriers coated with the thermoresponsive polymer (MMSN@TRP) were characterized (see supporting information and reference 26 for full characterization of each synthetic step). TEM images shows round-like shape particles with porous structure and SPIONs in their core (**Figure 1a**), while DLS measurements revealed a hydrodynamic size distribution shift up to 160 nm after the polymerization step (**Figure 1b**), which is in accordance with the polymer shell formation. A 20 % of weight loss measured by TGA is associated with the grafted polymer and the FT-IR revealed a band at 1650 cm^{-1}, which is characteristic of amide bond stretching ($\nu^{NC=O}$) band that confirms the presence of the polymeric shell in the device.

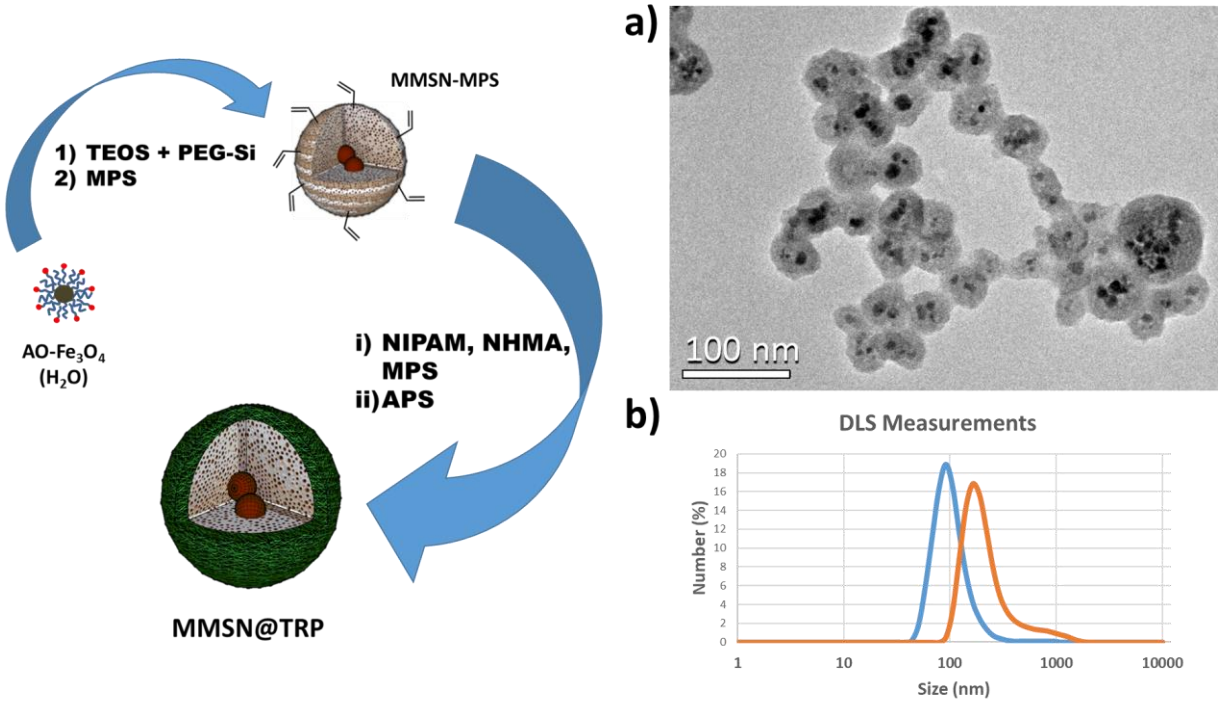

Figure 1. Scheme of the synthetic route of MMSN@TRP. a) TEM image of the nanocarriers coated with thermoresponsive polymer and SPIONS placed inside the silica matrix and b) hydrodynamic size of the precursor (MMSN-MPS, blue line) and the final nanocarrier (MMSN@TRP, orange line).

The iron determination revealed the ratio between the global material mass and the iron content, which is about 95.5 μg Fe·mg^{-1} material. The textural parameters and the magnetic heating properties were evaluated, confirming the drug loading capacity of the nanocarrier and a specific absorption rate (SAR) of 178,5 W·g Fe^{-1} as reported before,[38] which generates the required heat dissipation to reach the polymer shell and trigger the release mechanism. Also the drug loading capacity was estimated by UV vis measurements at 520 nm of the doxorrubicin loaded and empty nanocarrier at two different concentrations, showing a 2.5 % wt of drug cargo.

The experimental *in vivo* protocol to obtain the animal model is represented in the **Figure 2** and details are given in the experimental section. The selected tumor model is an allograft model

grown in a very commonly used immunocompetent mouse strain, C57/BL6. Most of the magnetic hyperthermia *in vivo* studies described in the literature use human tumor cell lines implanted in mice, i. e. xenograft tumor models, but this approach requires to use immunodeficient mice strains.[41–45] Although these are the easiest *in vivo* models for pre-clinical human tumors studies, they have the disadvantage of lacking the complete effect of the immune system. A deficient immune system, which usually plays a key role to combat diseases, could negatively influence the treatments underestimating the real effect. On the contrary, the selected tumor model, C57/BL6, has the advantage of a complete immune response but also some disadvantages, like having to use murine cells lines instead human cell lines, and the fact that allogaft tumor models usually grow very fast and the time window of study is limited, because usually the tumors ulcerate even when they are not very big.

One of the major problems to overcome when performing *in vivo* experiments using nanoparticles consists on the poor amount of material that reaches the desired location after systemic administration. And so it is when talking about the magnetic hyperthermia approach where the amount of magnetic material needed to release enough heat to kill cancer cells is usually high. This presents a real problem for many biological applications. Besides, there is a recent study that, after revising more than one hundred of papers, concluded that less than 1% of the intravenously administered dose arrives the tumor.[46] This is the reason why the majority of the published studies use the direct injection of the magnetic material at the tumor site as the main route of administration, trying to get the maximum MNPs content in the tumor site. However, this type of administration has the disadvantage that requires the establishment of subcutaneous tumors. Heterotopic tumors located outside the equivalent organ where the tumors should be grown, like subcutaneous implants, have the main drawback of having not a proper

tumor microenvironment. The interactions between the tumor and the surroundings affects tumor cell proliferation, levels of growth factors and nutrients, both during tumor angiogenesis and in its metastatic behavior. On the contrary, they have great advantages; they are very easy to handle and the good accessibility is of great help to assess the direct measurements to evaluate tumor growth progression. As can be seen in the **Figure 2** murine melanoma EL4 cells were injected subcutaneously in 7-week-old female C57BL/6 mice and after one week the tumors had the enough volume to be detectable and to be able to inject intratumor the nanocarrier.

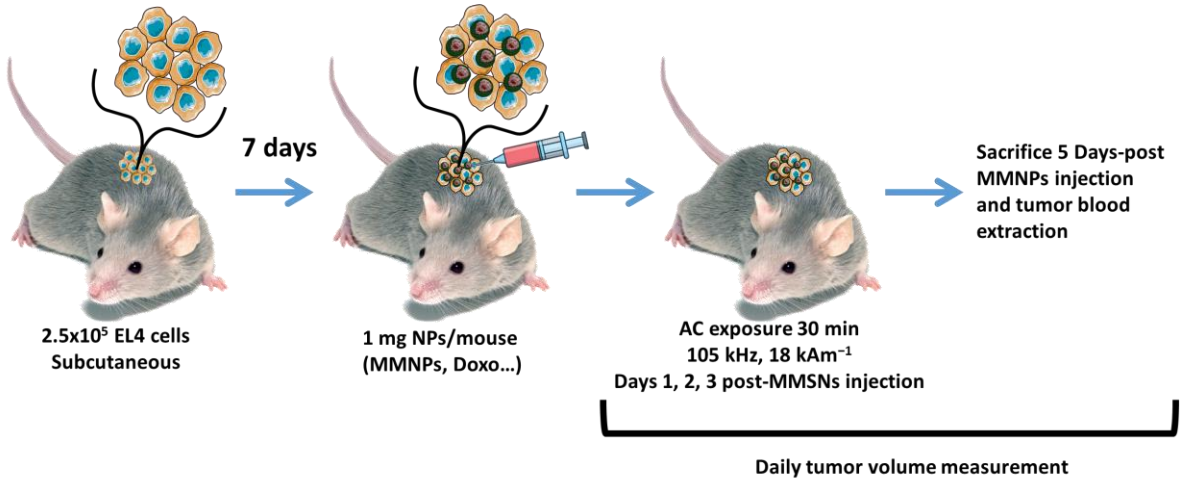

Figure 2. Scheme of the experimental protocol to obtain the tumoral animal model and details about the MNP injection and AMF exposition

Prior to the application of the treatment, the nanocarrier diffusion within the tumor tissue was tested with rhodamine tagged nanocarriers (MMSN-Rho@TRP). To make the device fluorescent, the surface of the uncoated MMSN-MPS precursor was decorated with APTES-modified rhodamine B isothiocyanate, which anchors to the nanoparticle by its silanol groups. Then, the radical polymerization was carried out with the fluorescent precursor, obtaining the same polymeric coating on the silica surface as obtained before. 1 mg of material, which corresponds to about 95.5 μg of Fe, was injected per mice of a group of three, and 96 hours after

the injection mice were euthanatized by CO_2 inhalation and the tumor was remove and fix in 4% of paraformaldehyde. The three tumors were prepared and ultrathin sections were stained with DAPI to study the penetration of the nanocarrier within the tumor. Even though the nanocarrier injection was performed just in one point of the tumor, they have deeply penetrated within the tumor as can be observed under confocal microscopy (**Figure 3**). Big accumulation is detected in two main regions, being the biggest one probably the injection point. It is appealing that the material is also easily found in the center of the tumor and even in the opposite edge. Therefore, the diffusion studies showed a remarkable tissue penetration for the polymeric coated nanocarrier.

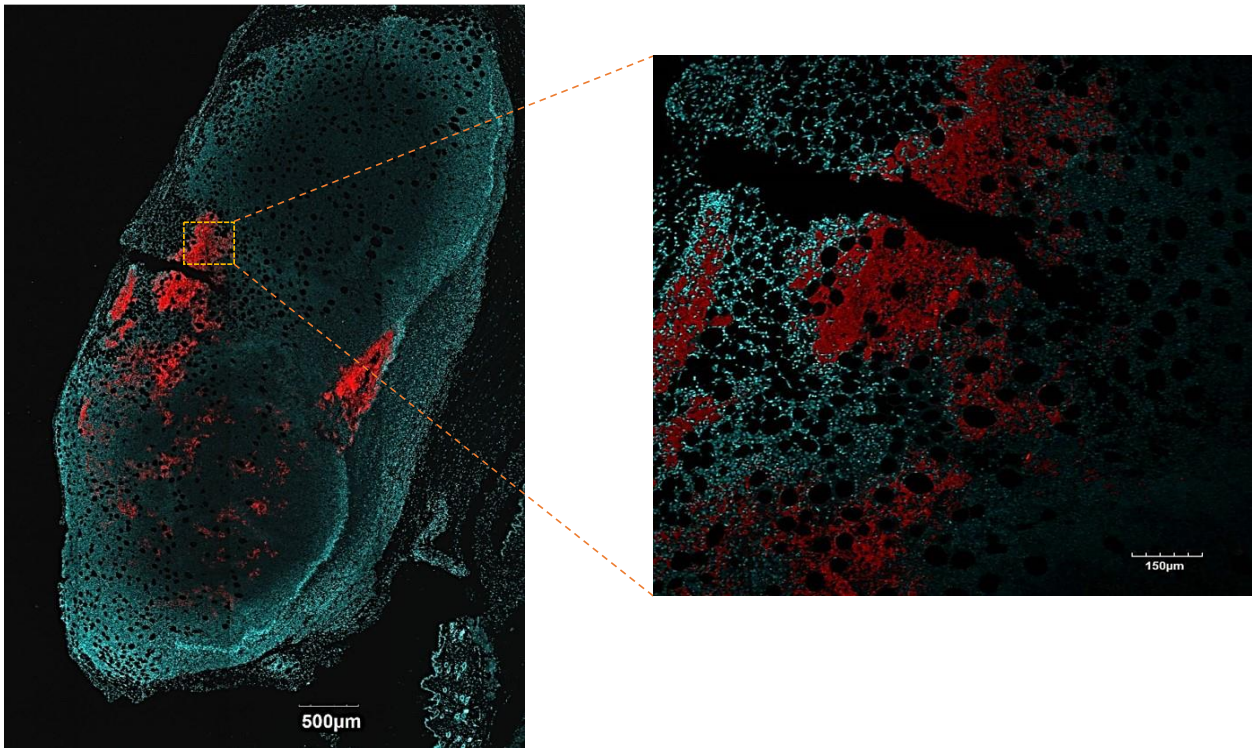

Figure 3. Confocal images of tumor slices after being stained with DAPI. Red fluorescence came from the Rho-nanocarriers.

Once the good penetrability of the material was confirmed, the following experiments were based on the application of the MH and the study of the tumor growth. Mice were divided

randomly in six different groups, each of them composed by four mice. To be able to detect and corroborate the synergistic effect between the heat release by the MMSNs and the drug release many controls were needed. A scheme of the experimental design can be seen in the **Figure 4**. Two control group which no particles and no free drug was injected, one without exposition to the AMF (A) and another under AMF application (B). Another two group of mice were injected with the doxorubicin loaded nanocarrier, one without AMF exposition (C) while the other group was exposed to the AMF (D). A fifth group of mice helped to the analysis of the tumor response to a free doxorubicin dose corresponding to a 100% release of the drug cargo from the device without AMF exposition (E). The last group of mice were injected with the unloaded MMSNs (without doxorubicin) and submitted to the AMF (E) to test the efficacy of the nanocarrier due to the heat generation *per se*. The MH treatment was applied in those pertinent groups for 30 minutes the day of the injection and two more consecutive days.

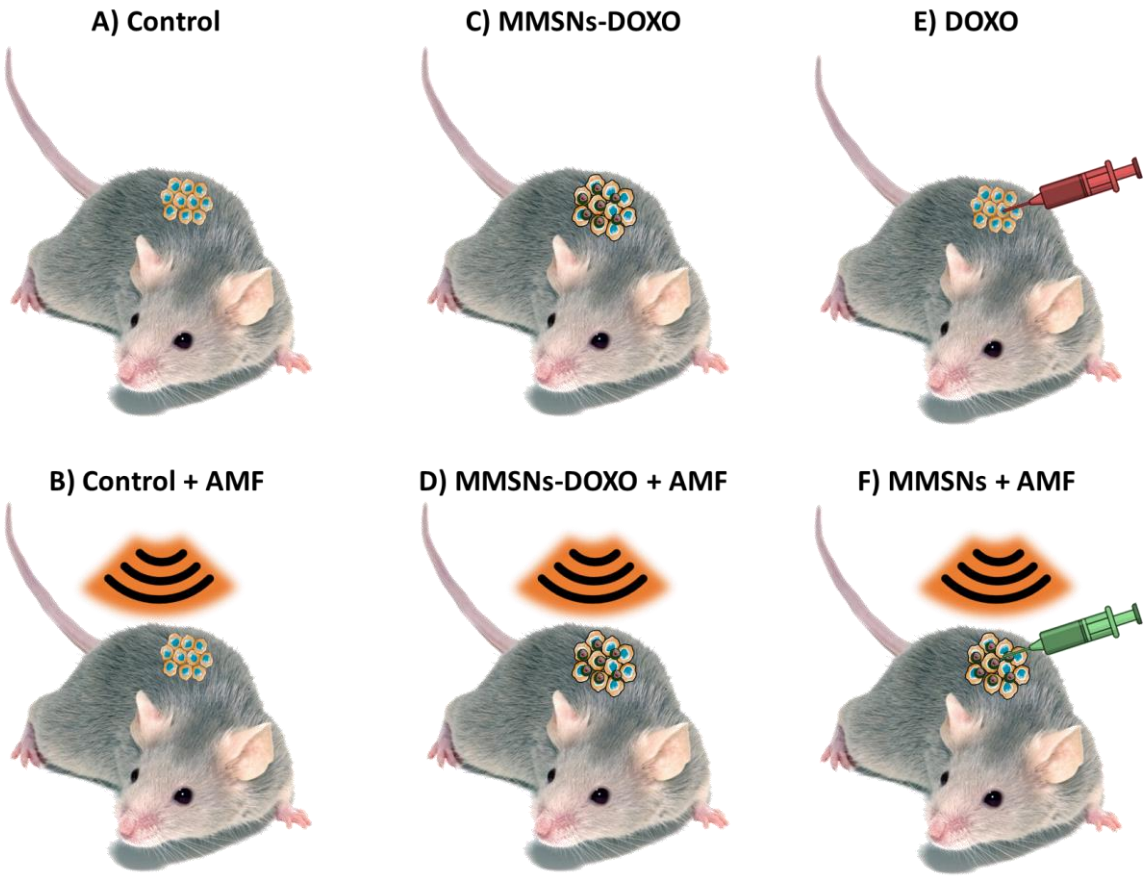

Figure 4. Experimental design of *in vivo* tests. A) Control group without AMF, B) control group with AMF, C) group with MMSNs-doxorubicin without AMF, D) group with MMSNs loaded with doxorubicin and exposed to AMF, E) group injected with free doxorubicin and F) group with MMSNs without doxorubicin exposed to AMF. Four mice composed each group.

It is worthy to briefly discuss the experimental conditions of the AMF applied due to there is an open debate about the biological safety limits for the amplitude and the frequency of the AMF. The heat generation caused by the eddy currents is non-selective heating, being therefore not useful for therapeutic purpose. The eddy currents occurred during an AMF application prompted to Atkinson et al to establish the first biological limit of the product $H \times f$ in 4.85 10^8 $Am^{-1}s^{-1}$ (where H is the amplitude and f the frequency of the magnetic field). Unlikely, this limit

was stated taking into account the general discomfort of patients that were receiving one hour of an AMF in the thorax area.[47] Later on, Hergt and Durtz estimated this limit up to 5 10^9 $A \cdot m^{-1}s^{-1}$ for smaller coils. Most of the published work about *in vivo* MH experiments set up the conditions between these two limits, but there are a considerable number of preclinical studies that use parameters above the upper limit. In our case, the H×*f* product gives a reasonable value of 1.89 10^9 $A \cdot m^{-1}s^{-1}$ which places this treatment below the upper limit,[48] having the possibility to enhance the antitumor efficacy by using 2-3 fold higher AMF parameters.

Animal weights and the three dimensions of the tumor, height (h), width (w) and length (l) were daily controlled, and the volume of the tumor was calculated as the volume of an ellipsoid using the following formula: $V= (\pi/6)\times h\times w\times l$. The tumor volume was monitored for each mouse every day of the treatment and normalized to the volume of the tumor the day of the MMSNs injection and first AMF application (day 1 in the experimental design) in order to evaluate the tumor growth. **Figure 5** shows the evolution of the mean of the body weight of all the animals in each experimental group along the complete experiment. The results indicate that there are no acute toxic effects coming from any of the elements of the complete treatment that provokes changes in the weight of the animals.

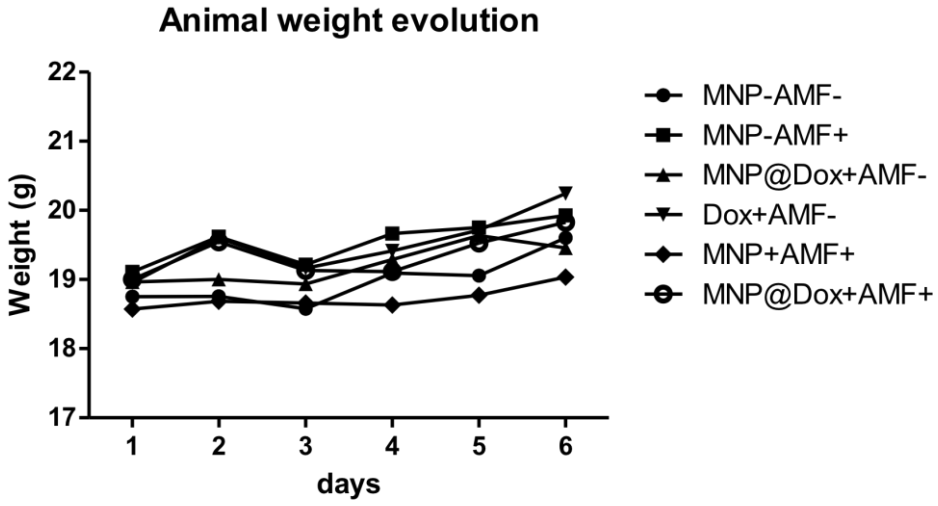

Figure 5. Mean of the weight of the animals along the experiment. (N=4, GraphPad Prism v5.03).

As can be seen in **Figure 6**, the Perls staining was also appropriate to detect de MNPs contained in the nanocarriers and therefore its penetration and distribution within the tumor in each single mouse which results to be very similar to the one observed in the **Figure 3** discussed above.

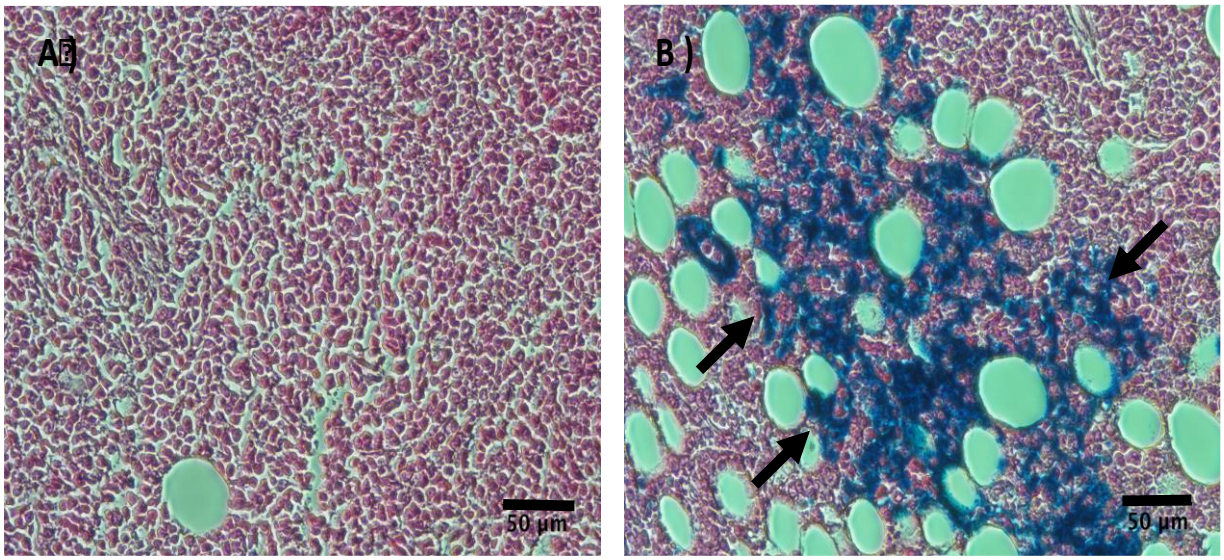

Figure 6. Perls staining (blue) of tumor slices from A) Control mice without nanocarriers and B) mice tumors injected with nanocarriers. Scale bar corresponds to 50 µm. In accordance with the diffusion studies, great results of tumor growth inhibition were obtained. Arrows indicate the presence of iron.

In **Figure 7** can be seen the tumor growth monitorization during the whole experiment, that is, from the first exposition to AMF to the mice sacrifice. There are no significant differences between the control groups and the group receiving the complete treatment at day 3, this is, the MMSNs heating and doxorubicin release after the last of the three consecutive MH applications. At the beginning of the experiment the tumor's volume duplicates just in 48h, giving an idea of

the aggressiveness of the tumor model commented previously. However, exciting results were obtained 48h after the last AMF exposure due to the tumor growth was deferred. A statistical significant difference ($p<0.001$) exists between all of the control groups and the group receiving the complete treatment. The tumor volume of all the controls was doubled from day 3 to day 5 whereas the tumor growth in the group with the complete treatment was inhibited.

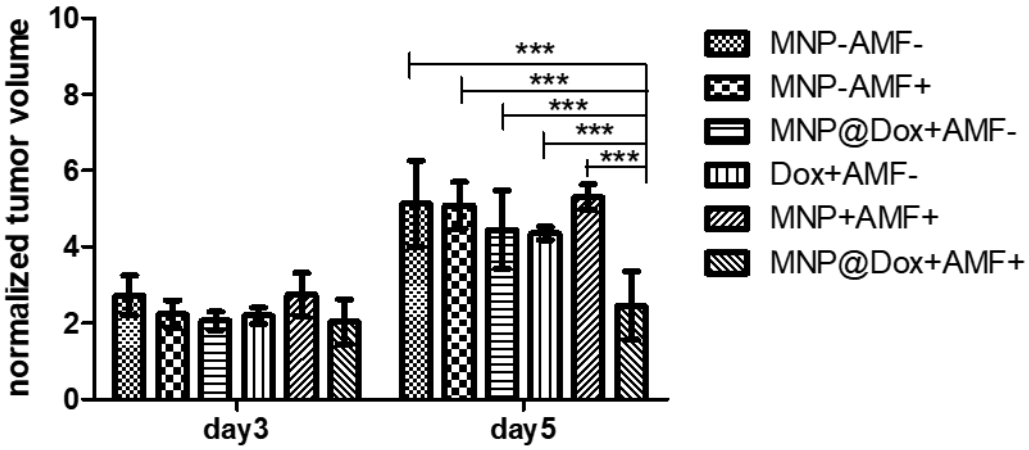

Figure 7. Tumor growth calculated as (Tumor Volume)/(Initial Tumor Volume). Day 3 corresponds to the measurements after the last magnetic hyperthermia treatment. Day 5 corresponds to 48h after the last magnetic hyperthermia treatment. N=4. *** $p<0.001$; two-way ANOVA, Bonferroni multiple comparison test.

The therapeutic effect demonstrates that the heating effect of the nanocarrier under AMF overcomes the heat dissipation of the blood stream *in vivo*, provoking the polymer transition and therefore the drug departure. The therapeutic efficacy also supports that the drug departure is taking place from the inside of the silica pore network only when AMF was applied; otherwise the Dox loaded sample counterpart (without AMF application) must have the same therapeutic effect. Remarkably, this point supports the synergic effect of chemotherapy and hyperthermia, because both control groups which have been treated with AMF only or doxorubicin only did not

show any tumoral growth inhibition effect. With these results it have been demonstrated that this nanocarrier has a powerful antitumor effect combining both the heat and the drug released by the MMSNs (despite the temperature rise was not evaluated in vivo).

The fact that none of the controls presented a growth inhibition effect is important indeed due to it implies an advantage over other systems in the literature that achieve the tumor growth inhibition in longer periods,[36] or require longer MH treatment periods,[44] even when a synergic treatment is applied.[43,49] These recent published works have also the need of heating at hyperthermia level the tumor tissue to obtain a significant tumor growth inhibition or regression. In our case the inhibition was observed 48 h after the last MH treatment. To study the growth inhibition effect at longer times an animal model with a slower tumor development can be used and therefore to enhance the final effect by several AMF expositions.

The absence of a growth inhibition effect in all the control groups can be based on the low amounts of nanocarrier used in this study. For that reason, the amount of injected drug has not a detectable effect or the drug leaking from the nanocarrier is blocked or very low without AMF revealing the absence of unspecific antitumor effect. Also the combination of a low amount of MMSNs and the type of AMF parameters did not provoke a global temperature increase that would produce *per se* a tumor growth inhibition. Finally, we can conclude that the proposed treatment could be a very useful tool to combat accessible tumors and there are still a lot of points of the approach that could be improved.

SUMMARY

In this work we study the final *in vivo* antitumoral effect of an innovative nanodevice under AMF treatment. This nanocarrier combines the heat release by magnetic nanoparticles and drug

release by a thermosensitive polymer. Evaluating the tumor growth, it has been demonstrated that there exists a synergistic effect between both the heat generation and the drug release. Interestingly, none of the controls, where the effect of single components was evaluated, produced any antitumor effect. It is worthy to mention that the AMF parameters used in this study are well below the biological safety limit of 5 10^9 $Am^{-1}s^{-1}$ and that the amount of MNPs injected per mice (182 μg Fe/tumor) is low in comparison with the majority of similar experiments published. That is why, these results are very promising and they confirm that there is no need to inject a huge amount of MNPs in the tumor in order to highly increases the macroscopic temperature to provoke antitumor effect, but taking advantage of the synergistic effect between a very localize heating and drug delivery is a very good strategy.

Despite the fact that there exist many knowledge gaps in the frame of *in vivo* MH applications, these results indicate that this nanocarrier and the proposed AMF treatment methodology have a great potential in the cancer treatment and it opens the possibility to further optimize and maximize the resulting treatment efficiency.

EXPERIMENTAL SECTION

Preparation of Hydrophobic Magnetite (OA-Fe_3O_4) NPs. Hydrophobic magnetite NPs were synthesized by one-pot chemical coprecipitation method. Deionized water was purged with nitrogen gas for 10 min. Then, 4.80 g of $FeCl_3$•6H2O, 2.00 g $FeCl_2$•4H2O, and 0.85 mL oleic acid were added to 30 mL of deionized water under nitrogen atmosphere with vigorous stirring. The mixture solution was heated to 90 ˚C. Then, 20 mL of ammonium hydroxide (14 wt %) was added rapidly to the solution, and it immediately turned black. The reaction was kept at 90 ˚C for 2.5 h and then allowed to cool to room temperature. The black precipitate was collected by

magnetic decantation and resuspended in chloroform with an end concentration of 62.6 $mg \cdot mL^{-1}$ oleic acid-capped Fe_3O_4.

Preparation of Mesoporous Magnetic Silica Nanoparticles (MMSNs). MMSNs were prepared through CTAB assisted iron oxide nanoparticle oil-to-water transfer followed by silica condensation a procedure described elsewhere. Briefly, 49.9 mg OA-Fe_3O_4 in $CHCl_3$ were poured (0.8 mL,0.04 $mL \cdot min^{-1}$ rate) into a recipient containing 580 mg of CTAB dissolved in 10 mL of H_2O (mQ) under mechanical stirring in an ultrasound bath. Once the removal of the organic solvent was completed, the dispersion was added to a 250 mL round-bottom flask with 86 mL NaOH (0.016M) solution at 45 ˚C and stirred at 600rpm. Then, the silica precursor mixture was added dropwise (1.2 mL of EtOH and 1 mL of TEOS at 0.25 $mL \cdot min^{-1}$ rate) and 15 min later, 260 µL of PEG-Si were added, and the suspension was stirred for 2h. The reaction mixture was washed with H_2O, and EtOH prior to the functionalization with 0.5 mL MPS in 150 mL of EtOH (99.5%) stirring at 35 ˚C during 16h. The surfactant template of the methacrylate functionalized MMSNs was removed by ion exchange using 150mL of 10 $g \cdot L^{-1}$ NH_4NO_3 in EtOH (95%) extracting solution during 2 h at 65˚C two times and the brown suspension was washed by several centrifugation and decantation steps with EtOH and keep it wet and sealed. The MMSN-MPS mass determination was done by drying an aliquot of the last wash step, and the so-obtained brown solid was used for characterization.

MMSNs Rhodamine labeling (MMSN-Rho). To anchor the dye to the MMSNs 2 mg of RITC were purged with nitrogen and 1 µL of APTES was added and stirred at r.t. during 1.5 h. At the same time, 150 mg of MMSN-MPS were centrifugated and the tube sealed to proceed with the N_2 purge for water removal before the addition of 10 mL of dry toluene and the dispersion carried to a flask under nitrogen flow. Once the reaction of the dye was completed the entire

reaction mixture was added to the flask and the temperature raised to 80 ˚C and stirred during 16 h. The excess of reactants was removed by washing one time with toluene and several times with ethanol until no dye is observed in the supernatant.

MMSNs Polymer Coating. 142.5 mg (1.26 mmol) of NIPAM, 12 mg of MBA (0.078mmol), 33.1 μL of NHMA (0.022 mmol, 48 %wt), 3.6 mg of CTAB and 5 mg of Na_2CO_3 were dissolved in 45 mL of water (mQ) and poured in a 100 mL three-neck round-bottom flask. The solution was stirred under N2 bubbling at 70 ˚C for 30 min to remove oxygen. Then, a dispersion of 50 mg of MMSNs dispersed in 5 mL of EtOH (99.5%) purged with N_2 was added to the monomer solution. The polymerization was initiated by the addition of 0.5 mL of a 10 $mg \cdot ml^{-1}$ APS solution in H_2O (mQ) previously deoxygenated to the reaction mixture. Ten minutes later the reaction mixture was allowed to cool down to room temperature and kept at that temperature overnight. The mixture was centrifuged and washed with THF twice and three more times with EtOH to remove the unreacted monomers and the organic solvent obtaining the thermoresponsive canocarrier MMSN@TRP.

MMSNs doxorubicin loading and drug cargo determination. Prior to the cargo loading the TR MMSN@TRP sample was washed with PBS (1x). Then, 50 mg of the solid were re-dispersed in a 1 $mg \cdot mL^{-1}$ solution of DOX in the same buffer and stirred for 24 h at 50 ˚C. The loaded MMSNs were washed by centrifugation with water and EtOH successively and dried in several aliquots under vacuum. For the DOX determination, two dispersions of the non-loaded (as a control) and drug-loaded nanocarriers at 0.1 $mg \cdot mL^{-1}$ and 0.5 $mg \cdot mL^{-1}$ were measured by UV-vis at 520 nm. The results were interpolated into a DOX standard fitting in PBS (1x) showing a 25 $\mu g \cdot mg^{-1}$ drug loading (2.5 % wt).

Cell line: EL4 murine lymphoma cell line from the strain C57BL/6N was cultured and maintained in RPMI1640 (Lonza) supplemented with 5% FBS () and 1% glutamine (Invitrogen) and 1% penicillin/streptomycin (Invitrogen). Cells were maintened in suspension in an incubator at 37ºC and in presence of 5% CO_2. Every two days the cell culture was diluted 1:10.

Animal model: Pathogen-free female 6-week C57BL/6 mice were commercially obtained from Charles River Laboratory and were maintained in the Animal facilities of the CIBA (IACS-Universidad de Zaragoza). Mice were held one week after arriving the animal facilities for acclimation. Animals were maintained according to the institutional animal use and care regulation of the Centro de Investigaciones Biomedicas de Aragón (CIBA, Zaragoza, Spain). All animal experiments were conducted according the law RD53/2013 and approved by the Ethics Committee for animal experiments from the University of Zaragoza that is an accredited animal-welfare body. After the week of acclimation, 2,5 10^6 EL4 cells suspended in 100 μL of sterile and complete culture medium without antibiotics were injected subcutaneously in the right flank of animals with a 25G needle. Before the injection the right flank of the animals was shaved. During the cells injection animals were anesthetized by inhalation of isoflurane (4% for the induction step and 2% for maintenance).

MH treatment: After 7 days of cell injection, tumors were small but big enough to be detected and to inject MMSNs intratumorally. Mice were randomnly divided in 6 groups of 4 mice each. In experimental groups with MMSNs (both with and without doxorubicin), 50 μL of sterile PBS containing 1mg of material were injected per mice (corresponds to about 182 μg Fe/tumor) with a 30G needle. MMSNs injection was performed in one point of the tumor. In control group with free doxorubicin mice were injected with 50 μL of 0,5 mg/mL doxorubicin in PBS (0,025 mg is the amount of doxorubicin calculated to be entrapted in 1 mg of material). The same day of

MMSNs injection and the following two days, mice were exposed to one AMF cycle. The device used for the AMF exposure was the model DM3 from nB nanoscale Biomagnetics (Zaragoza, Spain). Each exposure time was 30 min at 105 kHz and 18 $kA \cdot m^{-1}$. Mice were anesthetized with isoflurane and maintained during the AMF exposure onto a hot water bath system that prevents the mice to suffer hypothermia. Rectal temperature was registered during the AMF exposure to control general state of the animals. Tumor dimensions (length, with and height) and mice weight were daily measured with a Vernier. After the last AMF exposure mice were maintained 3 days or until tumors started to ulcerate.

Sample preparation and analyses: Mice were euthanasiated by CO_2 inhalation and blood was directly extracted from the heart and tumor was removed and fixed in 4% PFA and processed to perform three different staining: Hematoxylin/Eosin staining, DAPI and Blue Perls staining. All the sample preparation from the fixation on was made by the "Servicio Científico Técnico – Microscopía y Anatomía Patológica" of the CIBA (IACS-Universidad de Zaragoza). Samples were observed under an inverted microscope (Nikon eclipse TE2000-S) and using a confocal microscopy (Olimpus FV10-I Oil Type).

Characterization Techniques. Fourier transform infrared spectroscopy (FTIR) was carried out in a Thermo Nicolet nexus equipped with a Goldengate attenuated total reflectance device. Thermogravimetry analysis (TGA) were performed in a Perkin Elmer Pyris Diamond TG/DTA analyzer, with 5 °C min^{-1} heating ramps, from room temperature to 600 °C. The hydrodynamic size of mesoporous nanoparticles and SPION size were measured by means of a Zetasizer Nano ZS (Malvern Instruments) equipped with a 633 nm "red" laser. Transmission electron microscopy (TEM) was carried out with a JEOL JEM 2100 instruments operated at 200 kV, equipped with a CCD camera (KeenView Camera). Sample preparation was performed by

dispersing in MiliQ water ($CHCl_3$ for OA-Fe_3O_4) and subsequent deposition onto carbon-coated copper grids. UV-Vis spectrometry was used to determine the doxorubicin amount in the nanocarriers by means of a Biotek Synergy 4 device. Iron quantification for SAR measurements was determined by measuring the absorbance at 480 nm on a Thermo Scientific Multiskan GO UV/Vis microplate spectrophotometer after performing an acidic digestion and oxidation of the iron content of the material to Fe^{3+} and coupling it to 4,5-Dihydroxy-1,3-benzenedisulfonic acid disodium salt (TIRON, Sigma Aldrich) reagent. A calibration curve was performed following the same procedure using iron standard solution (Acros Organics) as reference. The SAR, measurements were performed on a DM100 system (nanoScale Biomagnetics) in the frequency range from 424 kHz to 838 kHz and magnetic fields of 20.05 to 23.87 $kA \cdot m^{-1}$. The textural properties of the materials were determined by nitrogen sorption porosimetry by using a Micromeritics ASAP 2020. To perform the N_2 measurements, the samples were previously degassed under vacuum for 24 h at room temperature.

Calculation Procedures: The SAR calculations were performed by DM100 system software (nanoScale Biomagnetics). All the statistics studies have been made using the GraphPad Prism v5.03 software. To calculate the p value the used test was two-way ANOVA, Bonferroni multiple comparison test. The surface area was determined using the Brunauer-Emmett-Teller (BET) method and the pore volume, Vpore ($cm^3 \cdot g^{-1}$), was estimated from the amount of N_2 adsorbed at a relative pressure around 0.99. The pore size distribution between 0.5 and 40 nm was calculated from the desorption branch of the isotherm by means of the Barrett-Joyner-Halenda (BJH) method. The mesopore size, Øpore (nm), was determined from the maximum of the pore size distribution curve.

AUTHOR INFORMATION

Corresponding Authors

E-mail: vallet@ucm.es, abaezaga@ucm.es

Present Addresses

† Dr. E. Guisasola is now located at CIC Biomagune, Paseo Miramón 182, 20009

Donostia/San Sebastián (Gipuzkoa)

Author Contributions

The manuscript was written through contributions of all authors. All authors have given approval to the final version of the manuscript.

Funding Sources

The present work was supported by grants from European Research Council (Advanced Grant VERDI; ERC-2015-AdG Proposal No. 694160) the Spanish MINECO project MAT2015-64831-R, SAF2014-54763-C2-2-R, Fondo Social de la DGA (grupos DGA) and COST Action TD1402 Radiomag

ACKNOWLEDGMENT

This work was supported by the European Research Council (Advanced Grant VERDI; ERC-2015-AdG Proposal No. 694160) and the project MAT2015-64831-R. LB thanks Santander-Universidad Zaragoza Fellowship program for her PhD position. LA thanks Juan de la Cierva Program for her postdoctoral possition. Authors would like to acknowledge the use of Servicios Científicos Técnicos del CIBA (IACS-Universidad de Zaragoza).

ABBREVIATIONS

MMSNs, magnetic mesoporous silica nanoparticles; AMF, alternating magnetic field; EPR, enhanced permeation and retention; MSNs, mesoporous silica nanoparticles; MNPs, magnetic nanoparticles; SPIONS, superparamagnetic iron oxide nanoparticles; MH, magnetic nanoparticles; OA, oleic acid; CTAB, hexadecyltrimethylammonium bromide; NIPAM, *N*-isopropylacrylamide; NHMA, *N*- (hydroxymethyl)acrylamide; MBA, *N, N'*-methylenebis(acrylamide); APS, ammonium persulfate; LCST, lower critical solution.

ASSOCIATED CONTENT

Additional characterization of the devices used in this work is supplied as Supporting Information. The full characterization can be found in reference 38.

REFERENCES

(1) Tibbitt, M. W.; Dahlman, J. E.; Langer, R. *J. Am. Chem. Soc.* **2016**, *138* (3), 704–717.

(2) Maeda, H.; Matsumura, Y. *Cancer Res.* **1986**, *46* (December), 6387.

(3) Maeda, H. *Adv. Drug Deliv. Rev.* **2015**, *91*, 3–6.

(4) Chen, B.; Dai, W.; He, B.; Zhang, H.; Wang, X.; Wang, Y.; Zhang, Q. *Theranostics* **2017**, *7* (73), 538–558.

(5) Yao, V. J.; D'Angelo, S.; Butler, K. S.; Theron, C.; Smith, T. L.; Marchiò, S.; Gelovani, J. G.; Sidman, R. L.; Dobroff, A. S.; Brinker, C. J.; Bradbury, A. R. M.; Arap, W.; Pasqualini, R. *J. Control. Release* **2016**, *240*, 267–286.

(6) Bertrand, N.; Leroux, J. C. *J. Control. Release* **2012**, *161* (2), 152–163.

(7) Vallet-Regí, M.; Rámila, A.; del Real, R. P.; Pérez-Pariente, J. *Chem. Mater.* **2001**, *13* (2), 308–311.

(8) Baeza, A.; Colilla, M.; Vallet-Regí, M. *Expert Opin. Drug Deliv.* **2015**, *12* (2), 319–337.

(9) Croissant, J. G.; Fatieiev, Y.; Almalik, A.; Khashab, N. M. *Adv. Healthc. Mater.* **2018**, *7* (4), 1700831.

(10) Rwei, A. Y.; Paris, J. L.; Wang, B.; Wang, W.; Axon, C. D.; Vallet-Regí, M.; Langer, R.; Kohane, D. S. *Nat. Biomed. Eng.* **2017**, *1* (8), 644–653.

(11) Martínez-Carmona, M.; Baeza, A.; Rodriguez-Milla, M. A.; García-Castro, J.; Vallet-Regí, M. *J. Mater. Chem. B* **2015**, *3* (28), 5746–5752.

(12) Mura, S.; Nicolas, J.; Couvreur, P. *Nat Mater* **2013**, *12* (11), 991–1003.

(13) Liu, Y.; Ding, X.; Li, J.; Luo, Z.; Hu, Y.; Liu, J.; Dai, L.; Zhou, J.; Hou, C.; Cai, K. *Nanotechnology* **2015**, *26* (14), 145102.

(14) Song, Y.; Li, Y.; Xu, Q.; Liu, Z. *Int. J. Nanomedicine* **2016**, *Volume 12*, 87–110.

(15) Tao, C.; Zhu, Y. *Dalt. Trans.* **2014**, *43* (41), 15482–15490.

(16) Yao, X.; Niu, X.; Ma, K.; Huang, P.; Grothe, J.; Kaskel, S.; Zhu, Y. *Small* **2017**, *13* (2), 1602225.

(17) Thomas, C. R.; Ferris, D. P.; Lee, J.-H.; Choi, E.; Cho, M. H.; Kim, E. S.; Stoddart, J. F.; Shin, J.; Cheon, J.; Zink, J. I. *J. Am. Chem. Soc.* **2010**, *132* (31), 10623–10625.

(18) Aznar, E.; Oroval, M.; Pascual, L.; Murguía, J. R.; Martínez-Máñez, R.; Sancenón, F. *Chem. Rev.* **2016**, *116* (2), 561–718.

(19) Hauser, A. K.; Wydra, R. J.; Stocke, N. A.; Anderson, K. W.; Hilt, J. Z. *J. Control. Release* **2015**, *219*, 76–94.

(20) Périgo, E. A.; Hemery, G.; Sandre, O.; Ortega, D.; Garaio, E.; Plazaola, F.; Teran, F. J. *Appl. Phys. Rev.* **2015**, *2* (4), 41302.

(21) Xu, Y.; Zhu, Y.; Kaskel, S. *RSC Adv.* **2015**, *5* (121), 99875–99883.

(22) Yu, X.; Zhu, Y. *Sci. Technol. Adv. Mater.* **2016**, *17* (1), 229–238.

(23) Tian, Z.; Yu, X.; Ruan, Z.; Zhu, M.; Zhu, Y.; Hanagata, N. *Microporous Mesoporous Mater.* **2018**, *256*, 1–9.

(24) Omar, H.; Croissant, J. G.; Alamoudi, K.; Alsaiari, S.; Alradwan, I.; Majrashi, M. A.; Anjum, D. H.; Martins, P.; Laamarti, R.; Eppinger, J.; Moosa, B.; Almalik, A.; Khashab, N. M. *J. Control. Release* **2017**, *259*, 187–194.

(25) Saint-Cricq, P.; Deshayes, S.; Zink, J. I.; Kasko, A. M. *Nanoscale* **2015**, *7* (31), 13168–13172.

(26) Baeza, A.; Guisasola, E.; Ruiz-Hernández, E.; Vallet-Regí, M. *Chem. Mater.* **2012**, *24* (3), 517–524.

(27) Guisasola, E.; Baeza, A.; Talelli, M.; Arcos, D.; Vallet-Regí, M. *RSC Adv.* **2016**, *6* (48), 42510–42516.

(28) Pradhan, P.; Giri, J.; Rieken, F.; Koch, C.; Mykhaylyk, O.; D??blinger, M.; Banerjee, R.; Bahadur, D.; Plank, C. *J. Control. Release* **2010**, *142* (1), 108–121.

(29) Nacev, A.; Weinberg, I. N.; Stepanov, P. Y.; Kupfer, S.; Mair, L. O.; Urdaneta, M. G.; Shimoji, M.; Fricke, S. T.; Shapiro, B. *Nano Lett.* **2015**, *15* (1), 359–364.

(30) Kim, J.; Piao, Y.; Lee, N.; Park, Y. Il; Lee, I. H.; Lee, J. H.; Paik, S. R.; Hyeon, T. *Adv. Mater.* **2010**, *22* (1), 57–60.

(31) Jordan, A.; Scholz, R.; Wust, P.; Fähling, H.; Roland Felix. *J. Magn. Magn. Mater.* **1999**, *201* (1–3), 413–419.

(32) Creixell, M.; Bohórquez, A. C.; Torres-Lugo, M.; Rinaldi, C. *ACS Nano* **2011**, *5* (9), 7124–7129.

(33) Asín, L.; Goya, G. F.; Tres, A.; Ibarra, M. R. *Cell Death Dis.* **2013**, *4* (4), e596–e596.

(34) Di Corato, R.; Béalle, G.; Kolosnjaj-Tabi, J.; Espinosa, A.; Clément, O.; Silva, A. K. A.;

Ménager, C.; Wilhelm, C. *ACS Nano* **2015**, *9* (3), 2904–2916.

(35) Brulé, S.; Levy, M.; Wilhelm, C.; Letourneur, D.; Gazeau, F.; Ménager, C.; Le Visage, C. *Adv. Mater.* **2011**, *23* (6), 787–790.

(36) Kossatz, S.; Grandke, J.; Couleaud, P.; Latorre, A.; Aires, A.; Crosbie-Staunton, K.; Ludwig, R.; Dähring, H.; Ettelt, V.; Lazaro-Carrillo, A.; Calero, M.; Sader, M.; Courty, J.; Volkov, Y.; Prina-Mello, A.; Villanueva, A.; Somoza, Á.; Cortajarena, A. L.; Miranda, R.; Hilger, I. *Breast Cancer Res.* **2015**, *17* (1), 66.

(37) Krawczyk, P. M.; Eppink, B.; Essers, J.; Stap, J.; Rodermond, H.; Odijk, H.; Zelensky, A.; van Bree, C.; Stalpers, L. J.; Buist, M. R.; Soullie, T.; Rens, J.; Verhagen, H. J. M.; O'Connor, M. J.; Franken, N. A. P.; ten Hagen, T. L. M.; Kanaar, R.; Aten, J. A. *Proc. Natl. Acad. Sci.* **2011**, *108* (24), 9851–9856.

(38) Guisasola, E.; Baeza, A.; Talelli, M.; Arcos, D.; Moros, M.; De La Fuente, J. M.; Vallet-Regí, M. *Langmuir* **2015**, *31* (46), 12777–12782.

(39) Lin, Y.-S. S.; Haynes, C. L. *Chem. Mater.* **2009**, *21* (17), 3979–3986.

(40) Lin, Y.-S.; Abadeer, N.; Haynes, C. L. *Chem. Commun.* **2011**, *47* (1), 532–534.

(41) Ling, Y.; Tang, X.; Wang, F.; Zhou, X.; Wang, R.; Deng, L.; Shang, T.; Liang, B.; Li, P.; Wang, D.; Ran, H.; Wang, Z.; Hu, B.; Li, C.; Zuo, G.; Zheng, Y. *RSC Adv.* **2016**, *7*, 2913–2918.

(42) Ohtake, M.; Umemura, M.; Sato, I.; Akimoto, T.; Oda, K.; Nagasako, A.; Kim, J. H.; Fujita, T.; Yokoyama, U.; Nakayama, T.; Hoshino, Y.; Ishiba, M.; Tokura, S.; Hara, M.; Muramoto, T.; Yamada, S.; Masuda, T.; Aoki, I.; Takemura, Y.; Murata, H.; Eguchi, H.; Kawahara, N.; Ishikawa, Y. *Sci. Rep.* **2017**, *7*, 1–12.

(43) Lin, W.; Xie, X.; Yang, Y.; Fu, X.; Liu, H.; Yang, Y.; Deng, J. *Drug Deliv.* **2016**, *23* (9),

3436–3443.

(44) Zhang, Z.; Song, S. *Biomaterials* **2017**, *132*, 16–27.

(45) Cheng, Y.; Muroski, M. E.; Petit, D. C. M. C.; Mansell, R.; Vemulkar, T.; Morshed, R. A.; Han, Y.; Balyasnikova, I. V.; Horbinski, C. M.; Huang, X.; Zhang, L.; Cowburn, R. P.; Lesniak, M. S. *J. Control. Release* **2016**, *223*, 75–84.

(46) Wilhelm, S.; Tavares, A. J.; Dai, Q.; Ohta, S.; Audet, J.; Dvorak, H. F.; Chan, W. C. W. *Nat. Rev. Mater.* **2016**, *1* (May), 1–29.

(47) Atkinson, W. J.; Brezovich, I. a; Chakraborty, D. P. *IEEE Trans. Biomed. Eng.* **1984**, *31* (1), 70–75.

(48) S, D. *J. Magn. Magn. Mater.* **2007**, *311*, 187.

(49) Guo, Y.; Zhang, Y.; Ma, J.; Li, Q.; Li, Y.; Zhou, X.; Zhao, D.; Song, H.; Chen, Q.; Zhu, X. *J. Control. Release* **2018**, *272*, 145–158.

Table of Contents

Tumor growth inhibition in vivo is achieved in 48 hours by a synergic effect between nanoscale hyperthermia and chemotherapy with magnetic-responsive mesoporous silica nanocarriers. The treatment is triggered by AMF application, and demonstrates that the nanocarrier heating overcomes the heat dissipation of the blood stream in vivo, provoking the polymer transition and therefore the drug release.

Keyword: hot spot, stimuli-responsive, drug delivery, magnetic hyperthermia

Eduardo Guisasola,[±] Laura Asín,[±] Lilianne Beola, Jesús M. de la Fuente, Alejandro Baeza* and María Vallet-Regí*

Title: Beyond Traditional Hyperthermia. In vivo Cancer Treatment with Magnetic-Responsive Mesoporous Silica Nanocarriers

ToC figure